8.16 PHYSICAL BIODYNAMICS

R. Ahmad, C. Beta, E. Bodenschatz, Z. Ditte, G. Eichele, A. Gholami, S. Goli Pozveh, A.-K. Günther, H.-F. Hsu, N. Kamprad, S. Kapoor, A. Krekhov, A. Pumir, V. Scheller, C. Schich, M. Tarantola, Y. Wang, C. Westendorf, V. Zykov

A. Bae (University of Rochester), J. Negrete jr. (MPI-KS, EPFL), R. Karmakar, E. Gutierrez, A. Groisman, W.-J. Rappel (University of California, San Diego)

In many cases an understanding of physical backgrounds of different biological processes is very important to optimise their dynamics or to prevent undesirable effects. In this chapter we consider examples of biodynamical processes including cilia driven flow in the brain, hydrodynamic interaction and waveform of oscillating flagellas, adhesion and migration of amoeboid cells, and spiral wave dynamics in excitable media.

8.16.1 Cilia-driven flows in the brain third ventricle

(Y. Wang, C. Westendorf) The cerebrospinal fluid (CSF) fills the cavities in the mammalian brain, known as the brain ventricular system, see Fig. 8.45(a). On a large scale the CSF is produced in a specialized tissue and then transported in a unidirectional manner from the lateral ventricles, through the third and fourth ventricle finally ending up and being reabsorbed in the spine. Almost all the surface of the ventricular system is covered with cilia bearing cells with the cilia often being arranged in bundles of up to 80 individual cilia. The continuous beating of these cilia bundles drives the CSF flow through the ventricular system. However, on a smaller scale, we have discovered that the cilia driven flow in the third ventricle (Fig. 8.45(a), green) is not a uni-directional throughflow but organized in rather complex flow patterns. Our initial analysis focused on the flow patterns itself and the polarization of the underlying tissue. We have extended the description onto several proteins, known as key players in establishing the planar cell polarity (PCP) of the tissue, as the orientation and location of the cilia bundles is likely tightly bound to the establishment of the PCP. After describing the flow patterns, we now ask the questions, how do these patterns arise during the development of the organism and which function may those patterns serve [1]. It is very intriguing to see, that comparing by now several hundreds of investigated specimens, the large-scale organization of the flow patterns and the underlying tissue polarization is remarkably conserved. We have therefore extended our studies to include the developmental timescale as an additional dimension describing the origin of the flow patterns. We hypothesize that the flow patterns serve for directed transport of signal molecules contained in lipid vesicles (exosomes). We thus applied injections of liposomes onto the prepared samples as a surrogate for the biological cargo. This allows for a much more accurate investigation of possible biological targets of the complex flow in the third brain ventricle, see

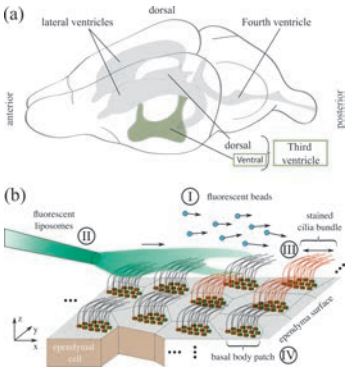

Figure 8.45: (a) Sketch of the mouse brain ventricular system with the ventral third ventricle colored in green. (b) Integrated approach to study the architecture and dynamics of local cilia arrangement. (I) - Bead tracking, (II) - Liposome injection, (III) - Live cilia staining, (IV) - Immunostaining.

Fig. 8.45(b). The entire project was carried out in a close collaboration with the department of Prof. G. Eichele at the neighboring MPIBC. This collaboration is now further intensified, as Prof. G. Eichele recently joined the MPI DS as an emeritus group with a fully equipped laboratory.

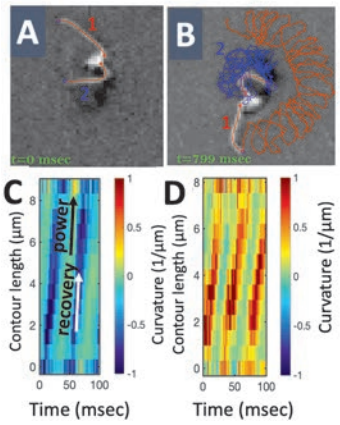

Figure 8.46: A swimming basal apparatus and the corresponding curvature waves propagating along each flagellum.

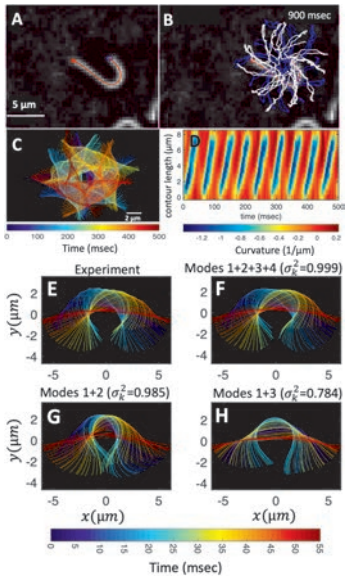

Figure 8.47: A-D) An isolated axoneme beating freely and rotating CCW. Curvature waves propagating along the contour length is also presented. E-H) Principal component analysis of the axonemal shapes.

8.16.2 *Resistive force theory and wave dynamics in swimming flagellar apparatus isolated from Chlamydomonas reinhardtii*

(A. Gholami) Cilia-driven motility and fluid transport is ubiquitous in nature and essential for many biological processes, including swimming of eukaryotic unicellular organisms. The-biflagellated micro-swimmer *Chlamydomonas reinhardtii* is a model organism to study dynamics of flagellar synchronization. Hydrodynamic interactions, intracellular mechanical coupling or cell body rocking are believed to play crucial role in synchronization of flagellar beating in green algae. We use freely swimming intact flagellar apparatus isolated from wall-less strain of *Chlamydomonas* to investigate wave dynamics. Our analysis in phase coordinates shows that, when the frequency difference between the neighboring flagella is high (10-41% of the mean), neither mechanical coupling via basal body nor hydrodynamics interactions are sufficiently strong to synchronize two flagella, indicating that beating frequency is perhaps controlled internally by the cell. We also examined the validity of resistive force theory for a flagellar apparatus swimming freely in the vicinity of a substrate and found a quantitative agreement between experimental data and simulations with drag anisotropy of ratio 2 (Fig. 8.46). Finally, using a simplified wave form, we have shown that by controlling phase or frequency differences between two flagella, steering can occur [2].

8.16.3 *On the existence of a back-propagating wave component in isolated Chlamydomonas reinhardtii flagella*

(A. Gholami) We also analyzed the motion of isolated and demembranated flagella from green algae *Chlamydomonas reinhardtii*, which act as ATP-driven micro-swimmers. The waveform of the *Chlamydomonas* beating flagella has an asymmetric waveform that is known to involve the superposition of a static component, corresponding to a fixed, intrinsic curvature, and a dynamic wave component traveling in the base-to-tip direction at the fundamental beat frequency, plus higher harmonics. We performed principal component analysis of the flagellar beat and show that the first four dominant eigenmodes describe the axonemal shapes with high accuracy. Furthermore, our mode analysis of free, pinned and clamped axonemes show the co-existence of a secondary tip-to-base wave component at the fundamental beat frequency that propagates opposite to the dominant base-to-tip wave, albeit with a smaller amplitude (Fig. 8.47). Finally, to understand the effect of calcium on the constituting wave components, we performed experiments at different [Ca^{2+}] and observed that as we increase [Ca^{2+}] from 0.0001

mM to 1 mM, the static mode drops significantly (∼ 85%), triggering a transition from circular swimming path to a straight trajectory [3].

8.16.4 *Cell adhesion and migration*

(A. Krekhov, M. Tarantola, C. Westendorf) Amoeboid adhesion is very versatile and does not involve focal adhesion complexes. We employed model substrates to identify adhesion mechanisms of the amoeba *Dictyostelium discoideum* (*D.d.*) and recently extended this approach to study contact guidance on micropatterned polyethylene-glycol gels, which nearly exclusively restrict migration to adjacent glass stripes. Surprisingly, this allowed us also to describe substantial differences between developmental stages and laboratory strains of *D.d.*, as also confirmed by single-cell adhesion force spectroscopy (SCFS) [4].

We furthermore studied the interplay of *D.d.* adhesion and Clathrin-Mediated-Endocytosis, which controls transmembrane protein recycling. We examined LimE-labelled actin foci cololcalized to spots of the adhesive protein SadA using a novel combination of SCFS and super-resolution microscopy (metal-induced energy transfer, MIET). We showed that the cell detachment process is sensitive to a loss of clathrin-light-chain (clc), reducing adhesion forces (Fig. 8.48A), number of adhesive points per cell and contact area. MIET allowed for quantification of the overall ventral height of carA-labelled cell membrane, clc, and actin relative to the underlying substrate (Fig. 8.48B-C). At actin foci locations coinciding with clc structures, the membrane is lifted and actin lifetimes increased. Cells deprived of clc show a significant reduction in actin-substrate distance (Fig. 8.48D) at increased foci densities. In summary, we can show that clc at actin foci is involved in cluster stability- and cell-substrate distance-regulation upon amoeboid cell adhesion [5, 6].

Besides the adhesome, the actin cytoskeleton and its response to external chemical stimuli is fundamental to amoeboid migration. One key player governing actin network dynamics is the motor protein myosin II. Based on experimental evidence, we have designed a model capturing three phases observed upon chemotactic stimulation by phase space embedding, which predicts a decreasing myosin II – actin coupling strength for the robust control of cell contraction upon chemotaxis [7].

D.d. cells also present other techniques to modulate the dynamical state of their actin cytoskeleton upon chemotaxis: In a population of cells, some specimen show noisy oscillatory cycles of actin polymerization, which we studied in response to external stimuli. These cells adopt a noisy quiescent state, before returning to their initial, oscillatory dynamics. We proposed a model based on a generic nonlinear noisy oscillator and a Hopf-bifurcation as transient termination mode [8].

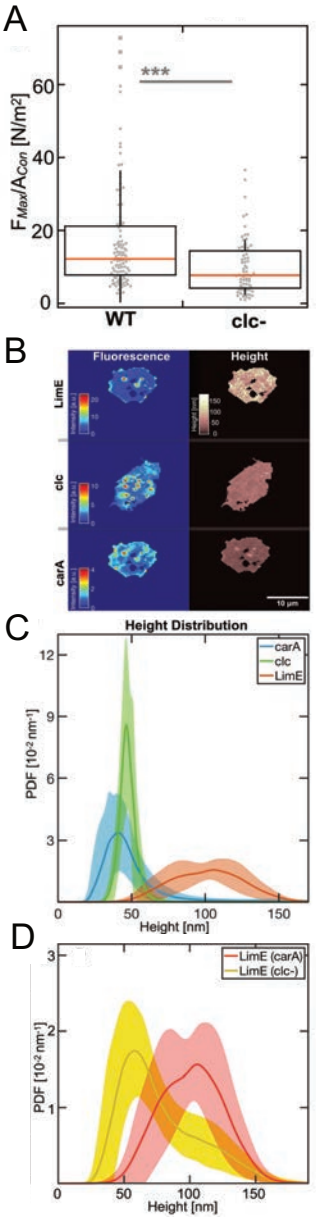

Figure 8.48: A: Maximum adhesion force F_{max} normalized to contact area for *D.d.* wild-type cells and amoeba with clc deletion. B. Exemplary cellular fluorescence (left) and MIET height (right) micrographs for: actin (LimE, top), clathrin (clc, middle) and membrane (carA, bottom) and corresponding average maps (+- SD) for WT (C)or clc null cells (D, shown only for LimE), n = 16-20 cells/category.

8.16.5 *Spiral waves within a bistability parameter region of an excitable medium*

(V. Zykov) Spiral waves are a prominent and intensively studied dynamic phenomenon in excitable media of very different nature. Until now, it has been assumed that an excitable medium must have a single stable resting state in order to sustain a spiral wave. Our computations, performed with the widely used Barkley model, clearly demonstrate that the spiral waves exist in a much wider parameter range than it was previously postulated in [9], as can be seen in Fig. 8.49.

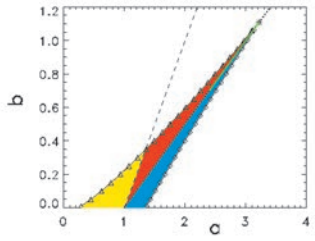

Figure 8.49: Parameter space of the Barkley model reads as $\partial u/\partial t = \nabla^2 u + u(u-1)[u - (v+b)/a]$, $\partial v/\partial t = \epsilon(u-v)$. There are no spiral waves within the white regions. The yellow region has been examined in [9]. The dashed line shows the boundary of the bistability region where $b < a - 1$. Within the red region, spiral waves rotate around a circular core. Within the blue region, spiral waves have a "negative" core. The dotted line shows the boundary between the positive and "negative" core regions expressed as $b = (a-1)/2$.

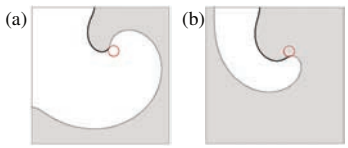

Figure 8.50: Counterclockwise rotating spirals with (a) positive and (b) "negative" core obtained for $a = 2.4$, $b = 0.7$ and $\epsilon = 0.02$. Within the gray regions $u(x,y,t) > 0.5$.

Within the bistability parameter region, where $b < a - 1$, no meandering spiral waves have been found. Here the spiral waves either rotate around a wave core that is at rest, or the tip trajectory orbits around a "negative" core that is located within the excited state. The obtained analytical expression $b = (a-1)/2$ for the boundary between these two parameter ranges is in quantitative agreement with the results of direct numerical computations [10].

Along the most part of this line, the core size is equal to zero. However, in the upper right part of this line, where $b > 0.7$, this solution becomes unstable. Depending on the initial conditions used, two different rotation patterns with a common positive or an unusual "negative" core are obtained here for the same parameter set, as shown in Fig. 8.50. Therefore, in this parameter range marked by the green line in Fig. 8.49, a duality of the spiral wave core and a hysteresis phenomenon in the spiral wave dynamics have been observed [10].

Thus, the calculations performed with the Barkley model allowed us to discover many important and unknown properties of rotating spiral waves. Since the Barkley model is very general and widely used to reproduce the basic properties of spiral wave dynamics, the data reported here should be applicable to various models and excitable media of different nature. We are planning to estimate parameters of the obtained spiral waves by application of the earlier elaborated kinematical approach [11].

It should be noted that spiral waves are considered as a plausible cause of cardiac arrhythmias, if the size of the heart muscle exceed at least the core diameter. From this point of view, the observed existence of spiral waves with an infinitely small core is rather important factor because a small core size obviously increases the probability of spiral wave maintenance.

[1] G. Eichele, E. Bodenschatz, Z. Ditte, A.-K. Guenter, S. Kapoor, Y. Wang, C. Westendorf, Phil. Trans. R. Soc. B **375**, 20190154 (2019)
[2] S. Goli Pozveh, A. Bae, A. Gholami, Soft Matter **17**, 1601 (2021)
[3] A. Gholami, R. Ahamd, A. Bae, A. Pumir, E. Bodenschatz, submitted (2021)
[4] R. Karmakar et al., PloS ONE **15**, e0236171 (2020)
[5] N. Kamprad, PhD thesis, University of Göttingen (2021)
[6] C. Schich, Master thesis, University of Göttingen (2020)
[7] H.-F. Hsu et al., New J. Phys. **21**, 113055 (2019)
[8] J. Negrete Jr et al., Phys. Rev. Res. **2**, 013239, (2020)
[9] S. Alonso, F. Sagues, A. S. Mikhailov, Science **299**, 1722 (2003)
[10] V.S. Zykov, E. Bodenschatz, submitted (2021)
[11] V.S. Zykov, in K. Tsuji and S. C. Mueller (eds.), Spirals and Vortices, Springer (2019)